

A limit analysis-based topology optimisation method for geostructure design

Xifan Li, Xue Zhang^{*}, Yujia Zhang

Department of Civil and Environmental Engineering, School of Engineering, University of Liverpool, Liverpool, UK

ARTICLE INFO

Keywords:

Topology optimisation
Limit analysis
Density-based method
Embankment
Soil foundation

ABSTRACT

Geostructures, vital for the progress of civilisation, often face inefficiencies and suboptimal performance due to the lack of optimisation in current designs. Achieving cost-efficiency in geostructure design involves optimising material usage while considering practical construction aspects. While size and shape optimisations are common in geostructure design, the application of topology optimisation remains underexplored. This paper addresses this gap by introducing a novel topology optimisation method for three-dimensional geostructure design. The method integrates mixed limit analysis and density-based topology optimisation theories, allowing for two-material design focused on the ultimate bearing capacity of the geostructure. The innovation resides in aligning the applied external load in the topology optimisation process with the ultimate load that the designed geostructure can sustain. The robustness of the proposed method is exemplified through its application to the design of an embankment and soil foundation, showcasing its potential to enhance the efficiency and performance of geostructures. This research contributes to the advancement of geostructure design practices, ultimately promoting sustainable and resilient infrastructure development.

1. Introduction

Geostructures play a key role in the advancement of human civilisation, providing essential support for buildings and transportation infrastructure. Despite their pivotal role, current designs of geostructures often lack optimisation, resulting in inefficiencies and suboptimal performance. Designing geostructures to be cost-efficient involves optimising material usage while considering practical construction aspects. However, achieving this balance is challenging due to the multitude of factors at play, encompassing geological, geotechnical, structural, and environmental considerations.

In geostructure design, conventional practices often rely on size and shape optimisations. Size optimisation aims to identify the optimal dimensions or scaling of structural elements while preserving the existing shape, while shape optimisation focuses on finding the optimal configuration of structural elements while maintaining a consistent size. Common structural elements in geostructure design include piles, shallow foundations, walls, anchors, among others. An alternative to these two methods is the topology optimisation, which optimises the spatial distribution of material within a specified domain. This is achieved by minimising a predefined cost function while meeting specified

constraints. Although topology optimisation is renowned for its efficiency in achieving optimal designs, its application in geostructure design remains underutilised with limited contributions specifically dedicated to its use in underground excavation (Ren et al., 2005, 2014) and foundation design (Kammoun et al., 2019, Pucker and Grabe, 2011, Seitz and Grabe, 2016). This is notably distinct from other engineering disciplines such as automotive engineering, aircraft engineering, and even structural engineering, where topology optimisation is actively employed to tailor structural designs optimally to problem-specific demands.

Several topology optimisation approaches have been devoted over the past few decades (Sigmund and Maute, 2013). Among them, the density-based topology optimisation method, particularly the so-called Solid Isotropic Material with Penalization (SIMP) method, stands out as widely adopted. The traditional SIMP method involves minimising the elastic strain energy of a structure subjected to specified external loads, a volume constraint, and assumptions of linear elastic material behaviour. This approach found practical application in the field of geotechnical engineering, specifically in the design of foundation structures, as demonstrated by Pucker and Grabe (2011). Despite the widespread use of the traditional SIMP method in structural

^{*} Corresponding author.

E-mail address: xue.zhang2@liverpool.ac.uk (X. Zhang).

optimisation, designs obtained through this approach may not ensure the feasibility of stress states in relation to material strength. In simpler terms, the optimised design generated by the traditional SIMP method does not guarantee that the stress states within the structure remain below the yield limit of the material when subjected to the considered external loads. This raises concerns about the structural integrity and performance of the designed system in real-world conditions. The stress-constrained topology optimisation method was proposed to address this issue (Duysinx and Bendsoe, 1998), wherein stress constraints are additionally incorporated. Remarkably, linear elastic structural analysis continues to be utilised in the traditional stress-constrained topology optimisation, notwithstanding the added stress constraints (Holmberg et al., 2013). This persistence results in a conservative design, as demonstrated in the work of Zhang et al., (2023a) and Li et al. (2023). An alternative approach, which considers stress, is the topology optimisation method for stiffness and strength. Functioning as a hybrid method, it seeks to minimise both the compliance of a structure and the homogenisation of stresses and was recently applied in the design of strip foundations (Hadjiloo et al., 2023).

In a recent development, Kammoun and Smaoui (2015) proposed a density-based topology optimisation formulation that integrates limit plasticity. This method, grounded in lower bound finite element limit analysis, ensures the preservation of a statically admissible stress field throughout the optimisation process, thereby facilitating the determination of a structure's ultimate plastic limit. Subsequently, Herfelt et al. (2019) introduced an alternative plasticity-based formulation that enables both upper and lower bound finite element limit analysis using different elements. However, their formulation produces designs solely in greyscale. To overcome this limitation, Zhang et al., (2023a) introduced a penalty into the framework proposed by Herfelt et al. (2019), allowing for the creation of black-and-white designs. It is also demonstrated that the formulation proposed in the work of Zhang et al., (2023a) does not require a stress-relaxation technique. Li et al. (2023) further extended the work specifically for three-dimensional scenarios involving mesh refinement techniques. Alternatively, Mourad et al. (2021) introduced a formulation for topology optimisation incorporating plastic limit analysis. Diverging from the previously mentioned approaches (Herkfelt et al., 2019; Kammoun and Smaoui, 2015; Li et al., 2023; Zhang et al., 2023a), Mourad et al. (2021) aims to maximise the load-bearing capacity of the structure. This is accomplished while considering material strength properties and adhering to a material volume constraint.

This paper aims to develop a tailored topology optimisation method for designing three-dimensional geostructures, with a emphasise on achieving the design's limit state. To fulfill this goal, the devised method integrates both mixed limit analysis theory and density-based topology optimisation theory. It accommodates two materials, such as soils and foundations/reinforcements, and incorporates gravity effects into the topology optimisation process. The ultimate formulation seeks to minimise the volume of material used for foundations or reinforcement, considering yielding states of both soil and foundations/reinforcements. To validate the proposed method, the geostructure resulting from the developed method is extracted for bearing capacity analysis. Additionally, a comparative analysis between the performance of designs derived from our approach and those using traditional geotechnical practices was conducted to illustrate the robustness and efficiency of our method.

The rest of the paper is structured as follows. Section 2 introduces the theory of mixed limit analysis. Section 3 presents the plasticity-based topology optimisation formulation for two-material design. Numerical examples are illustrated in Section 4 with conclusions drawn in Section 5.

2. Mixed limit analysis formulation

In this section, we provide a summary of the formulation for mixed limit analysis. The mixed formulation incorporates both displacement

and stress as variables, as introduced by Krabbenhöft et al. (2007), and operates within the framework of the generalized Hellinger Reissner variational principle proposed by Zhang et al. (2019). Specifically, a mixed limit analysis formulation is expressed as a min–max optimisation problem:

$$\begin{aligned} \min_u \max_{(\sigma, \alpha)} \quad & \alpha + \int_{\Omega} \sigma^T \nabla^T(\mathbf{u}) d\Omega - \alpha \int_{\Gamma_t} \bar{\mathbf{t}}^T \mathbf{u} d\Gamma - \int_{\Omega} \mathbf{b}^T \mathbf{u} d\Omega \\ \text{subject to} \quad & f(\boldsymbol{\sigma}) \leq 0 \end{aligned} \quad (1)$$

where $\boldsymbol{\sigma} = (\sigma_{xx} \ \sigma_{yy} \ \sigma_{zz} \ \sigma_{yz} \ \sigma_{zx} \ \sigma_{xy})^T$ represents the Cauchy stress, \mathbf{u} denotes the displacement, \mathbf{b} is the body force, $\bar{\mathbf{t}}$ is the prescribed traction, $f(\boldsymbol{\sigma})$ is the yield function, α is the collapse load factor (e.g., $\alpha\bar{\mathbf{t}}$ indicating the ultimate force the structure can sustain), and ∇ is the differential operator matrix.

In 3D cases, when employing a four-node tetrahedron, the approximation of displacement (\mathbf{u}) within an element is expressed as:

$$\mathbf{u}(\mathbf{x}) \approx N\hat{\mathbf{u}} \quad (2)$$

where $\hat{\mathbf{u}}$ comprises the displacement values at mesh nodes, and N represents the shape function. Accordingly, the strain is approximated by:

$$\boldsymbol{\varepsilon} \approx \nabla^T(N\hat{\mathbf{u}}) = \mathbf{B}\hat{\mathbf{u}} \quad (3)$$

with $\mathbf{B} = \nabla^T N$ being the strain–displacement matrix. Sequentially, the min–max problem (1) is discretised as

$$\begin{aligned} \min_{\hat{\mathbf{u}}} \max_{(\sigma, \alpha)} \quad & \alpha + \int_{\Omega} \sigma^T \mathbf{B} d\Omega \hat{\mathbf{u}} - \alpha \int_{\Gamma_t} \bar{\mathbf{t}}^T N d\Gamma \hat{\mathbf{u}} - \int_{\Omega} \mathbf{b}^T N d\Omega \hat{\mathbf{u}} \\ \text{subject to} \quad & f(\boldsymbol{\sigma}) \leq 0 \end{aligned} \quad (4)$$

where $\boldsymbol{\sigma}$ represents the uniform stress in the integral domain. The minimisation part of (4) can be resolved analytically, leading to a subsequent maximisation problem which is

$$\begin{aligned} \max_{(\sigma, \alpha)} \quad & \alpha \\ \text{subject to:} \quad & \int_{\Omega} \sigma^T \mathbf{B} d\Omega = \alpha \int_{\Gamma_t} \bar{\mathbf{t}}^T N d\Gamma + \int_{\Omega} \mathbf{b}^T N d\Omega \\ & f(\boldsymbol{\sigma}) \leq 0 \end{aligned} \quad (5)$$

The mixed limit analysis formulation mentioned above has been integrated into the finite element limit analysis commercial software OptumG2/G3. In the implementation, the finite elements utilised assume a quadratic displacement field and a linear stress field. It is noteworthy that the occurrence of volumetric locking is evident when employing elements with linear shape functions, for instance three-node triangular elements in 2D cases and four-node tetrahedral elements in 3D cases. To tackle this issue, this study incorporates nodal integration based on smoothing domains, also referred to as cells, following the work of Zhang et al. (2023b). The construction of cells involves dividing each tetrahedron into four hexahedrons (see Fig. 1(a)), ensuring equal volumes, by connecting the centroid of the tetrahedron to the centroids of the four surface triangles and then the centroid of each surface triangle to the three mid-edge nodes of the triangle. The cell associated with a node comprises all hexahedrons adjacent to that specific node. Fig. 1(b) illustrates a cubic domain discretised using cells. For further insights into the construction of smoothing domains/cells, interested readers are directed to the work of Li et al. (2023) and Zhang et al. (2023b). It has been demonstrated that the volumetric locking issue associated with linear elements can be effectively overcome by employing this approach (Meng et al., 2020; Zhang et al., 2023b).

Following nodal integration, maximisation problem (5) is written as

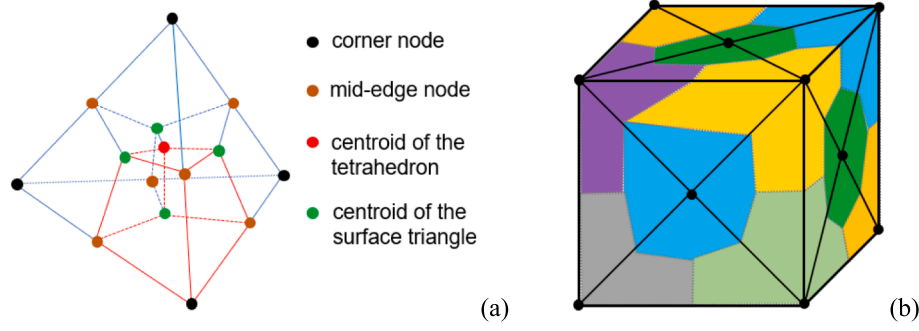


Fig. 1. Illustrations of 3D cell construction: (a) A tetrahedron divided into four hexahedrons, and (b) the cell generated based on tetrahedrons for a cube (Zhang et al., 2023b).

$$\begin{aligned} & \max_{(\hat{\sigma}, \alpha)} \quad \alpha \\ & \text{subject to:} \quad \begin{cases} \bar{\mathbf{B}}^T \hat{\boldsymbol{\sigma}} - \bar{\mathbf{F}}_b = \bar{\mathbf{F}}_t \\ f^i(\hat{\boldsymbol{\sigma}}) \leq 0 \quad i = 1, 2, \dots, NN \end{cases} \end{aligned} \quad (6)$$

in which the notation $(\bullet)^i$ denotes the value of (\bullet) at the i th node unless otherwise specified, NN represents the total number of nodes (equal to the total number of cells, NC). The vector $\hat{\boldsymbol{\sigma}}$ comprises stress components at all mesh nodes and can be viewed as a weighted average stress of the tetrahedrons adjacent to each node.

The global matrix $\bar{\mathbf{B}}^T$ is computed by

$$\bar{\mathbf{B}}^T = \int_{\Omega} \mathbf{B}^T d\Omega = \sum_{i=1}^{NN} \left(\frac{1}{V^i} \sum_{j=1}^{ne} \left(\frac{1}{4} \mathbf{B}_{ij}^T V^j \right) \right) \quad (7)$$

where $\sum(\bullet)$ denotes the standard finite element assembly operator, V^i is the volume of the i th cell, V^j is the volume of the j th tetrahedron, ne is the total number of tetrahedron elements adjacent to the i th node, and \mathbf{B}_{ij} is the strain–displacement operator at the i th node contributed by the j th adjacent tetrahedron. Hence, $\frac{1}{V^i} \sum_{j=1}^{ne} \left(\frac{1}{4} \mathbf{B}_{ij}^T V^j \right)$ represents the weighted average of the strain–displacement operator at the i th node.

The surface force and body force are $\bar{\mathbf{F}}_t$ and $\bar{\mathbf{F}}_b$, respectively, whose estimates based on nodal integration are

$$\bar{\mathbf{F}}_t = \alpha \int_{\Gamma_t} \bar{\mathbf{t}}^T N d\Gamma = \alpha \sum_{i=1}^{NN} \beta_t^i \left(\bar{\mathbf{t}}^i \Gamma^i \right) \quad (8)$$

and

$$\bar{\mathbf{F}}_b = \int_{\Omega} \mathbf{b}^T N d\Omega = \sum_{i=1}^{NN} (\mathbf{b}^i V^i) \quad (9)$$

in which Γ^i is the nodal contour area, and β_t^i is a factor that equals one if the node belongs to a Neumann boundary and zero otherwise.

It is worth highlighting that, even in the absence of an upper/lower bound feature in the abovementioned mixed limit analysis, the solution derived from such analysis often closely approximates to the exact bearing capacity of a structure, as indicated by Nguyen (2023).

3. Topology optimisation formulation for two-material structures

3.1. Single-material structure design

Li et al. (2023) indicated that the topology optimisation with plasticity can be formulated as a volume minimisation problem through the introduction of a novel design variable, ‘density’ (denoted as $\rho \in [0, 1]$), in problem (6). The modified optimisation problem takes the form:

$$\begin{aligned} & \min_{(\hat{\boldsymbol{\sigma}}, \hat{\boldsymbol{\rho}})} \quad \mathbf{L}^T \hat{\boldsymbol{\rho}} \\ & \text{subject to:} \quad \begin{cases} \bar{\mathbf{B}}^T \hat{\boldsymbol{\sigma}} - \bar{\mathbf{F}}_b \hat{\boldsymbol{\rho}} = \bar{\mathbf{F}}_t \\ f^i(\hat{\boldsymbol{\sigma}}, \hat{\boldsymbol{\rho}}) \leq 0 \quad i = 1, 2, \dots, NN \end{cases} \end{aligned} \quad (10)$$

where $\hat{\boldsymbol{\rho}} = [\rho_1, \rho_2, \dots, \rho_{NN}]^T$ represents a vector containing the ‘density’ (ρ) at all nodes, and $\mathbf{L} = [V_1, V_2, \dots, V_{NC}]^T$ is a vector comprising the volumes of all cells. In the work of Li et al. (2023), only one material is considered in the optimal design. Thereby, $\rho_i = 0$ in problem (10) implies that the i th cell is a void. In this study, the von Mises model is employed as the plasticity model for clay. The yield condition of von Mises provides a smooth approximation of the Tresca yield condition, which has been widely embraced for the analysis of clay in undrained conditions (Dunne and Martin, 2017, Walker and Yu, 2010, Zhang et al., 2023b). When using the von Mises yield criterion, the inequality constraint in problem (10) is expressed as:

$$f^i = \sqrt{3J_2} - \rho_i f_y \leq 0 \quad (11)$$

where $J_2 = \frac{1}{6}(\sigma_x - \sigma_y)^2 + \frac{1}{6}(\sigma_y - \sigma_z)^2 + \frac{1}{6}(\sigma_z - \sigma_x)^2 + \sigma_{xy}^2 + \sigma_{yz}^2 + \sigma_{zx}^2$ is the second invariant of the deviatoric stress, and f_y is the yield stress of the material. In the case of single material topology design, the modified yield criterion (11) is supplemented with an additional inequality condition:

$$f_{sp}^i = |\sigma_x + \sigma_y + \sigma_z| - k f_y \rho_i \leq 0 \quad (12)$$

to prevent a spherical stress state (e.g., $\sigma_x = \sigma_y = \sigma_z$) when $\rho_i = 0$.

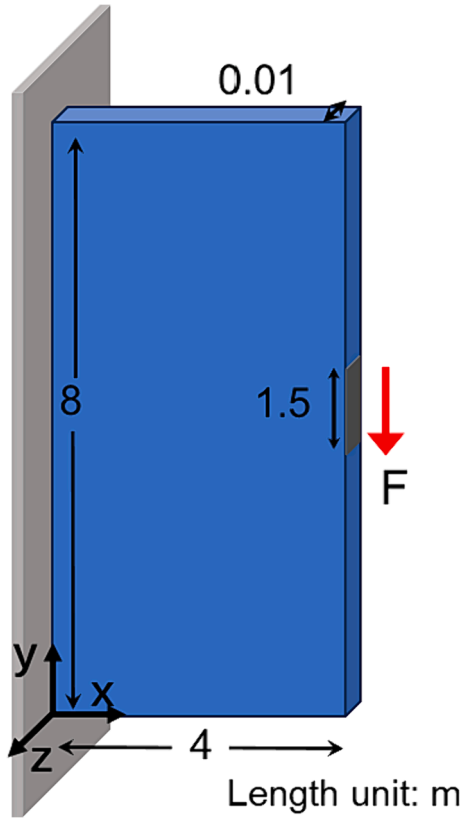


Fig. 2. A plate under shear stress.

3.2. Two-material structure design

In this section, the scope of problem (10) will be generalised to incorporate two-material topology optimisation. In other words, the space can be either occupied by clays or foundations/reinforcements. To this end, the Von Mises yield criterion at the i th node/cell thereby should be modified as:

$$f^i = \sqrt{3J_2} - \rho_i f_{y1} - (1 - \rho_i) f_{y2} \leq 0 \quad (13)$$

where f_{y1} and f_{y2} represent the yield stress of foundations/reinforcements and clays, respectively. Specifically, the i th cell is occupied by foundations/reinforcements with yield stress f_{y1} if $\rho_i = 1$, and by clays with yield stress f_{y2} if $\rho_i = 0$. When $f_{y2} = 0$, inequality (13) simplifies to the optimal design scenario for a single material structure, for instance, the condition outlined in (11). Given the binary occupation of space by either foundations/reinforcements or clays in a two-material structure design, the inclusion of the additional inequality constraint (12) is unnecessary in this study.

Additionally, the term related to the body force should be adjusted. For two-material structure design, the gravitational component should be expressed as

$$\begin{aligned} \int_{\Omega} [\rho_i \mathbf{b}_1 + (1 - \rho_i) \mathbf{b}_2] N d\Omega &= \sum_{i=1}^{NN} [\rho_i \mathbf{b}_1 + (1 - \rho_i) \mathbf{b}_2] V^i \\ &= \sum_{i=1}^{NN} (\mathbf{b}_1^i V^i - \mathbf{b}_2^i V^i) \rho_i + \sum_{i=1}^{NN} (\mathbf{b}_2^i V^i) \end{aligned} \quad (14)$$

in which, \mathbf{b}_1 and \mathbf{b}_2 denote the body forces of clays and foundations/reinforcements considered in the design.

Consequently, the topology optimisation formulation for two-material structure design is presented as

$$\begin{aligned} &\min_{(\hat{\sigma}, \hat{\rho})} L^T \hat{\rho} \\ &\text{subject to: } \begin{cases} \bar{\mathbf{B}}^T \hat{\sigma} - \hat{\mathbf{F}}_b \hat{\rho} = \bar{\mathbf{F}}_t + \tilde{\mathbf{F}}_b \\ f^i(\hat{\sigma}, \hat{\rho}) = \sqrt{3J_2} - \rho_i f_{y1} - (1 - \rho_i) f_{y2} \leq 0 \\ 0 \leq \rho_i \leq 1 \quad i = 1, 2, \dots, NN \end{cases} \\ &\text{where } \begin{cases} \bar{\mathbf{B}}^T = \sum_{i=1}^{NN} \left(\frac{1}{V^i} \sum_{j=1}^{nc} \left(\frac{1}{4} \mathbf{B}_j^T V^j \right) \right) \\ \hat{\mathbf{F}}_b = \sum_{i=1}^{NN} (\mathbf{b}_1^i V^i - \mathbf{b}_2^i V^i) \\ \bar{\mathbf{F}}_t = \alpha \sum_{i=1}^{NN} \beta_{\Gamma}^i \left(\hat{\mathbf{t}}_n \Gamma^i \right) \\ \tilde{\mathbf{F}}_b = \sum_{i=1}^{NN} (\mathbf{b}_2^i V^i) \end{cases} \end{aligned} \quad (15)$$

The optimisation formulation presented in (15) results in a grayscale solution. To achieve a black-and-white design, it is necessary to penalise

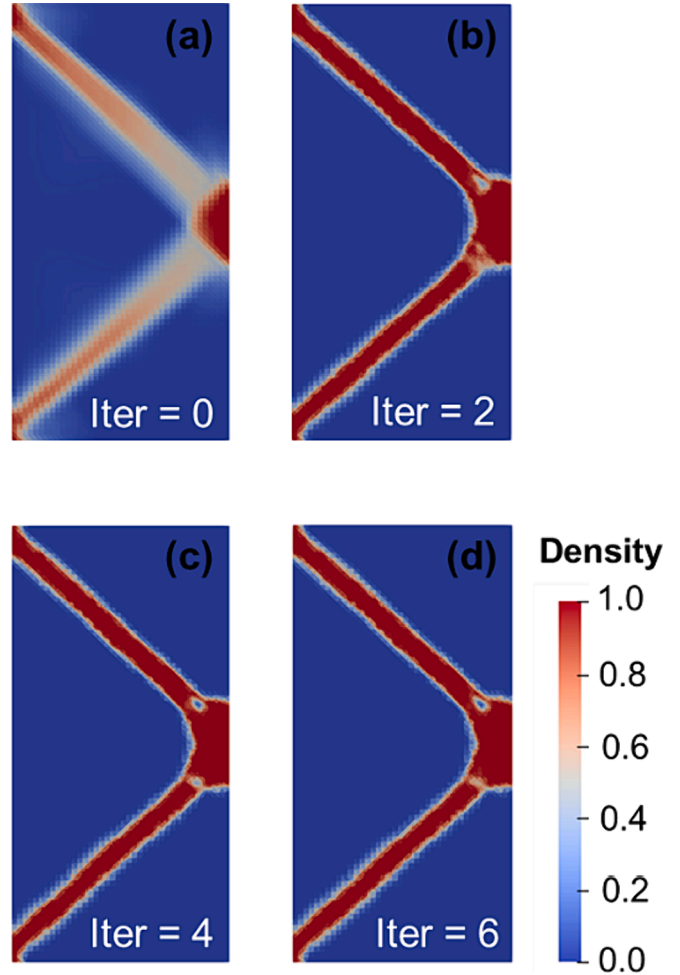


Fig. 3. The evolution of material distributions with iteration number (a) iter = 0; (b) iter = 2; (c) iter = 4; and (d) iter = 6, where ‘density’ $\rho = 0$ represents MA, and $\rho = 1$ represents MB, reflecting the optimisation process.

the objective function. In line with the approach detailed in previous works of Kammoun et al. (2019), Zhang et al., (2023a), and Li et al. (2023), the vector L is substituted with $\tilde{L} = [c_1 V_1, c_2 V_2, \dots, c_{NC} V_{NC}]^T$, where the penalty factor for the i th node, c_i , is determined by

$$c_i = e^{p(1-\rho_i^*)} \quad (16)$$

in which ρ_i^* denotes the ‘density’ at the i th node obtained in the previous iteration, and p is a constant set to 5 as suggested by Li et al. (2023), if not otherwise specified. The effectiveness of this exponential penalty function has been investigated in previous studies conducted by Smaoui and Kammoun (2022) and Zhang et al., (2023a).

Consequently, the plasticity-based topology optimisation for two-material structures can be expressed as:

$$\begin{aligned} & \min_{(\hat{\sigma}, \hat{\rho})} \quad \tilde{L}^T \hat{\rho} \\ & \text{subject to: } \left\{ \begin{array}{l} \bar{B}^T \hat{\sigma} - \hat{F}_b \hat{\rho} = \bar{F}_t + \tilde{F}_b \\ f^i(\hat{\sigma}, \hat{\rho}) = \sqrt{3}J_2 - \rho f_{y1} - (1 - \rho)f_{y2} \leq 0 \\ 0 \leq \rho_i \leq 1 \quad i = 1, 2, \dots, NN \end{array} \right. \\ & \text{where } \left\{ \begin{array}{l} \tilde{L}^T = [c_1 V_1, c_2 V_2, \dots, c_{NC} V_{NC}] \\ \bar{B}^T = \sum_{i=1}^{NN} \left(\frac{1}{V_i} \sum_{j=1}^{nc} \left(\frac{1}{4} B_j^T V_j \right) \right) \\ \hat{F}_b = \sum_{i=1}^{NN} (b_1^i V_i - b_2^i V_i) \\ \bar{F}_t = \alpha \sum_{i=1}^{NN} \beta_i^i \left(\tilde{t}_n^i \Gamma^i \right) \\ \tilde{F}_b = \sum_{i=1}^{NN} (b_2^i V_i) \end{array} \right. \quad (17) \end{aligned}$$

The optimisation problem (17) can be redefined as a conventional standard second-order cone programming (SOCP) problem following the work of Meng et al. (2020) and Zhang et al. (2023a). The resolution of this SOCP problem is accomplished by MOSEK (ApS, 2019), a comprehensive optimisation software designed for addressing linear, quadratic, conic, semidefinite, and mixed integer problems, among others.

A common numerical instability encountered in topology optimisation is the checkerboard phenomenon. A standard method to enhance numerical stability involves the use of the checkerboard-filtering method. In this study, we employ the density filtering method suggested by Sigmund (2007) that the filtered density at the i th point is computed as:

$$\tilde{\rho}_i = \frac{\sum_{j \in N_n} w(x_j) V_j \rho_j}{\sum_{j \in N_n} w(x_j) V_j} \quad (18)$$

Here, V_j represents the volume of the j th cell, ρ_j is the ‘density’ at the j th node, and N_n denotes the total number of nodes within the filtering region of the i th node. The filtering region is defined as a circle with a radius of R . The weighting function, denoted as $w(x_i)$, takes the form of a Gaussian (bell shape) distribution function, as in the work of Sigmund (2007):

$$w(x_j) = e^{-\frac{1}{2} \left(\frac{\|x_j - x_i\|}{\sigma_d} \right)^2} \quad (19)$$

in which x_i denotes the coordinates of the i th node undergoing density filtering, and x_j represents the coordinates of the j th nodes within the filtering region. The effectiveness of the aforementioned weighting function in plasticity-based topology optimisation has been demonstrated in prior studies for single-material design in both 2D (Zhang et al., 2023a) and 3D (Li et al., 2023) scenarios. In this study, the same weighting function is utilised for two-material topology optimisation. The parameter σ_d in Eq. (19) is set to the value of $R/2$, where R is 1.5 times the mesh size, aligning with the recommendation provided by Zhang et al. (2023a).

Given that the objective function incorporates an exponential penalty function of the ‘density’, achieving a converged solution necessitates an iterative approach as outlined by the subsequent steps:

- (i) **Initialisation:** Start by assuming an initial ‘density’, $\rho = 1$, for all nodes in the domain.
- (ii) **Penalty Factor Calculation:** Compute the exponential penalty factor, c_i , for each node using Eq. (16).
- (iii) **Optimisation Problem Solving:** Utilise the MOSEK solver to solve the optimisation problem (17) which couples the limit analysis and density-based topology optimisation, thereby obtaining the density field and stress field.
- (iv) **Density Filtering:** Apply density filtering (e.g., using Eq. (18)) and consider the filtered value as the updated density for each node.
- (v) **Convergence Check:** Evaluate the convergence criterion. Terminate the iteration if the criterion is met; for example, if the change in the objective function, $Obj = \tilde{L}^T \hat{\rho}$, between two consecutive iterations satisfies $\frac{\|Obj_{n+1} - Obj_n\|}{Obj_{n+1}} \leq \text{tolerance value}$. If not, proceed to step (ii) and repeat the entire process until the convergence criterion is satisfied.

Notably, both the objective function and the constrains in (15) are linear. Consequently, the optimisation problem can be categorised as mathematically convex. Therefore, it can generally be anticipated that the optimisation result is a global solution. Nonetheless, with the introduction of the penalty factor c_i , which is contingent upon the density from the preceding iteration step, the resultant binary design from the above iterative procedure may not necessarily represent a global minimum.

4. Numerical examples

In this section, three examples are provided to validate the proposed method and demonstrate its robustness in geostucture design. All simulations were conducted on a DELL PC with a 2.20 GHz CPU and 32.0 GB memory running Microsoft Windows Server (Version 11.0). The final SOCP problem is resolved using MOSEK (ApS, 2019), an advanced modern optimisation tool for addressing large-scale optimisation problems, in MATLAB environment (R2022b).

4.1. Design of a short plate

To validate the proposed method, we first examine the design of a short plate, as depicted in Fig. 2. The plate dimensions are 4 m \times 8 m \times 0.01 m. The left surface of the plate is fully fixed, while the front and back surfaces are fixed in the z direction. The plate is designed to experience a vertical shear load of 227 kPa distributed over a 1.5 m central section on its right surface.

Two materials can be used in the design of this plate: Material A (MA) with a yield stress of 30 kPa, and Material B (MB) with a yield stress of

300 kPa. Given that MB is much more expensive than MA, we are expected to minimise the use of MB while ensuring that the designed plate can sustain the given shear load.

Fig. 3 illustrates the evolution of material distribution through various iterations. It is evident that a highly diffuse structure is achieved when no iteration is conducted (Fig. 3(a)). Because of the application of penalisation, an almost binary material structure emerges through subsequent iterations (Fig. 3 (b)–(d)). As shown, with increasing iterations, the plate’s domains are predominantly occupied by either MA ($\rho = 0$) or MB ($\rho = 1$), with very few domains exhibiting $0 < \rho < 1$. The material layouts after 4 iterations (Fig. 3(c)) and 6 iterations (Fig. 3(d)) closely resemble each other, indicating a converged solution. This convergence aligns with the trend observed in the volume ratio of MB (e.g., the ratio of the volume of MB to the total volume of the plate) against iteration number, as illustrated in Fig. 4. After 4 iterations, the volume ratio of MB stabilises, showing minimal change and converging to a value of 16.5 %.

Notably, this study incorporates the mesh refinement technique introduced by Li et al. (2023) for enhancing computational efficiency. The fundamental concept of this technique involves refining meshes in the domain with a density greater than a specified value, such as 0.3 in this study. The simulation begins with 6,642 nodes and 19,200 elements. As the simulation progresses, both the number of nodes and elements gradually increase, reaching 10,671 nodes and 37,808 elements, respectively. Following this point, these quantities remain constant. The total computation time for this particular case, involving a total of 10 iterations, amounts to 243 s. This refinement results in a very thin transition area from a density of 0 to a density of 1, as illustrated in Fig. 5 (a). For validation purposes, a binary material structure is extracted from Fig. 5(a), as shown in Fig. 5(b). Utilising the commercial software OptumG2, the maximum shear load that this structure can sustain is determined to be 230 kPa, which closely matches the external shear load value of 227 kPa applied in the initial topology optimisation simulation. This alignment demonstrates the accuracy and validity of the proposed method.

4.2. Embankment design

Earthen embankments play a crucial role in civil engineering infrastructures, serving to control flooding and provide support for various overlying transport structures. A recent focus has been on exploring biopolymer-treated soil for constructing embankments, aiming to address challenges such as mitigating internal erosion and enhancing stability (Chang et al., 2020). In this section, we will apply the developed topology optimisation approach to design an embankment using

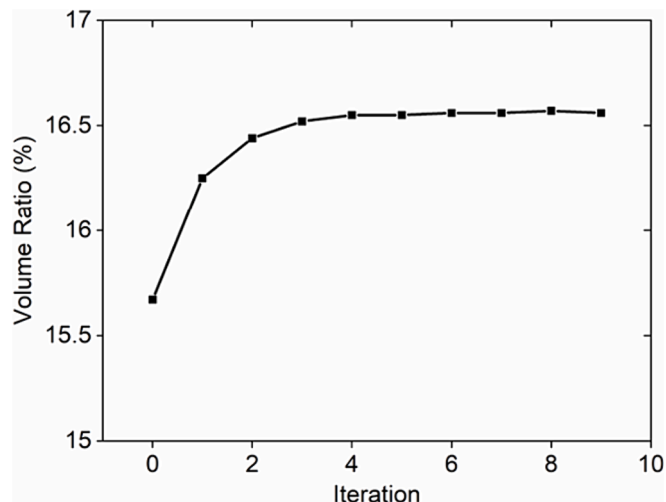


Fig. 4. The curve of volume ratio of Material B (MB) against iteration number.

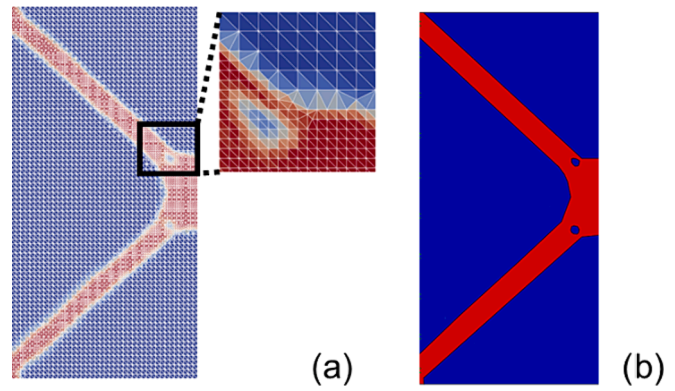


Fig. 5. The illustration of (a) the converged material layout with meshes and (b) the extracted binary-material structure.

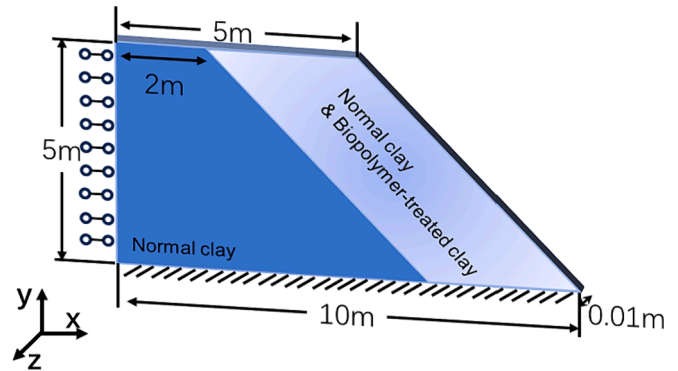


Fig. 6. Schematic diagram of an embankment.

biopolymer-treated clays, ensuring it meets the required Factor of Safety.

The schematic representation of the embankment is depicted in Fig. 6, with only one-half simulated owing to its symmetrical nature. The bottom of the embankment is fully fixed, while symmetric boundary conditions are imposed on the left surface. The front and back surfaces are fixed in the z direction, mimicking a plane strain condition. The embankment will be constructed using normal clays with a bulk unit weight of 19.6 kN/m³ and a cohesion of 30 kPa, and biopolymer-treated clays with a bulk unit weight of 27.5 kN/m³ and a cohesion of 230 kPa – values falling within the reported range (Chang et al., 2020). When utilising only normal clays in the construction, the Factor of Safety (FoS) for the constructed embankment is 2.87. In this study, we will explore how to further incorporate the minimal biopolymer-treated clays into the construction, ensuring a FoS of 4.0. The domain allowed to use biopolymer-treated clays is in a shape of parallelogram (i.e., the light blue region indicated in Fig. 6), referred to as design domain. In this study, the yield stress f_y of clays is twice the value of the cohesion, implying that the von Mises yield surface middle circumscribes the Tresca yield surface. Additionally, the yield stress to be used in the topology optimisation process should be f_y/FoS to ensure the required FoS. In the simulation, a fine mesh with a mesh size of $h_e = 0.1$ m is employed to discretise the region where biopolymer-treated clay can be applied. In contrast, a relatively coarse mesh with $h_e = 0.2$ m is utilised in the remaining area. This configuration yields a total of 10,908 nodes and 55,152 elements. Without further refinement of the meshes in the simulation, the computational cost amounts to 335 s, allowing for the attainment of a converged solution over 9 iterations.

Fig. 7 shows the evolution of material distribution across different iteration steps. Like the first example, an initially diffuse distribution is achieved without iteration. However, after undergoing 9 iterations, the

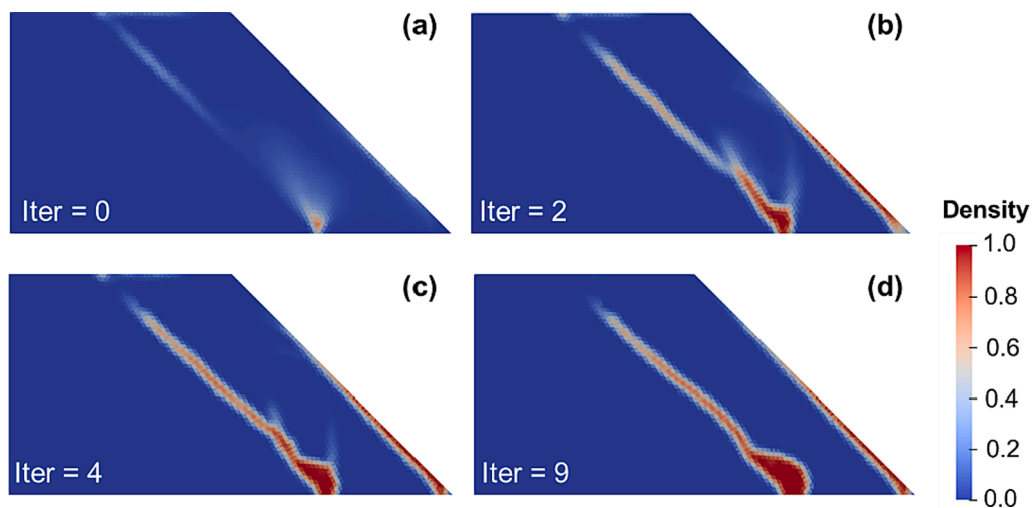


Fig. 7. The evolution of material distributions for the embankment with iteration number (a) iter = 0; (b) iter = 2; (c) iter = 4; and (d) iter = 9, where ‘density’ $\rho = 0$ represents normal clays, and $\rho = 1$ represents biopolymer-treated clays.

material distribution transforms into a nearly binary state, yielding a biopolymer-treated clay volume ratio of 6.1 %. Most biopolymer-treated clays (i.e., red part in Fig. 7(d)) are concentrated along the left and right surfaces of the design domain (i.e., the parallelogram). A notable quantity of these clays is also found in the bottom-left corner of the design domain. Stability analysis of the embankment design resulting from the topology optimisation was conducted using the commercial software OptumG2. In the analysis, both the normal clay and biopolymer-treated clay were treated as rigid-perfectly plastic materials. Specifically, the Drucker-Prager (DP) model in OptumG2 was employed. The two strength parameters associated with the DP model are $M = 0$ and $k = 2c/\sqrt{3}$ where c is the cohesion for normal clay (30 kPa) and biopolymer-treated clay (230 kPa). Consequently, the values of parameter k for normal clay and biopolymer-treated clay are 35 kPa and 266 kPa, respectively. With such settings, the DP model in OptumG2 degrades to a von Mises model with the yield surface middle circumscribing the Tresca yield surface, ensuring that the material model used in the stability analysis remains consistent with that utilised in the

topology optimisation simulation. Whilst the geometry remains constant for the stability analysis, it is imperative to extract interface information to differentiate between the domains occupied by normal and biopolymer-treated clays. The identification of interfaces entails discerning boundaries between domains with densities exceeding and falling below 0.5. This geometric and interface data is then utilised to construct the analysis model in OptumG2, with corresponding material parameters, such as unit weight and cohesion, allocated to the respective domains to facilitate the analysis. Nodes and elements are automatically generated in OptumG2 utilising mesh adaptivity technique, thereby guaranteeing the achievement of converged solutions. Fig. 8 illustrates the stability analysis results from OptumG2. The FoS of the embankment with biopolymer-treated clays is 3.946, in agreement with the expected FoS. Compared to the embankment constructed using just normal clay (Fig. 8(a)), fewer soils are disturbed when the embankment with biopolymer-treated clays fails (Fig. 8(b)). This is attributed to the presence of the biopolymer-treated clays on the far left of the design domain, causing the shear band to propagate on its right.

It is notable that the shape of the region designated for biopolymer-treated soil exhibits irregularity, which poses significant challenges for practical engineering implementation. Hence, it is advisable to slightly simplify the derived optimal topology to yield a more practical and easily implementable soil distribution for engineering purposes. This adaptation ensures that the insights gained from the optimisation process are translated into feasible engineering solutions. Table 1 illustrates the designed simplified from our topology optimisation solution and three other designs influenced by traditional reinforcement approaches. These conventional strategies include the integration of reinforced materials at the base, the implementation of ecological blankets, and their synergistic combinations. All designs maintain a consistent area occupied by biopolymer-treated soils, approximately 2.29 m², reflecting a 6.1 % volume ratio of biopolymer-treated clays achieved from our topology optimisation. Table 1 reveals that the design strategy inspired by combining ecological blanket implementation and toe reinforcement (type 3) yields the highest FoS (3.756) among the three designs emulating conventional reinforcement strategies. Nevertheless, this FoS is still lower than that of the embankment design simplified from our topology optimisation solution (i.e., type 4), standing at 3.896. This underscores the effectiveness of the proposed method for embankment design.

4.3. Soil foundation

In the last example, we explore the design of a soil foundation as

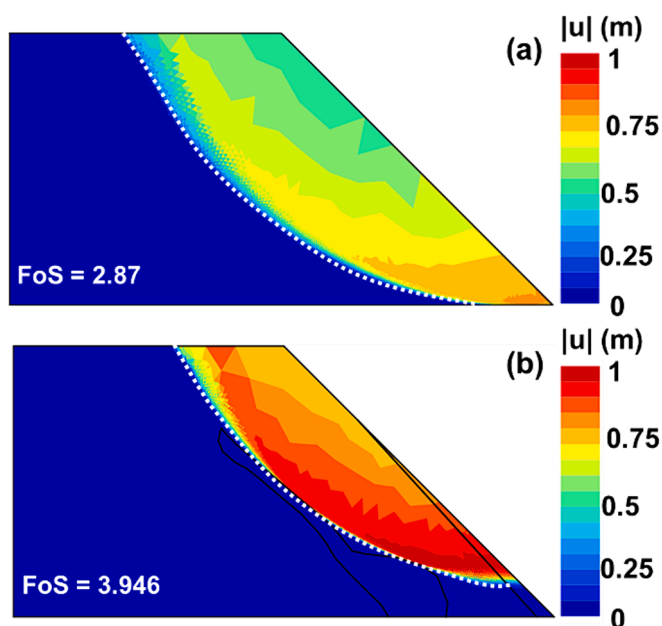

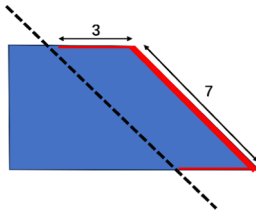
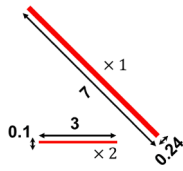
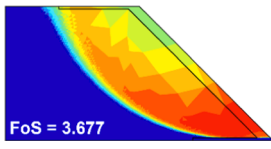
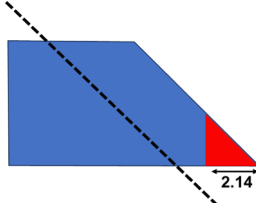

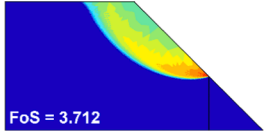
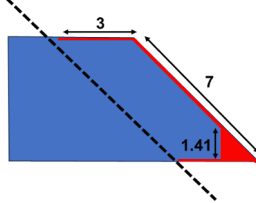
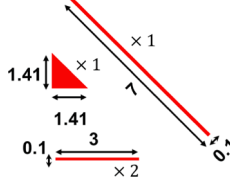
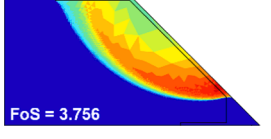
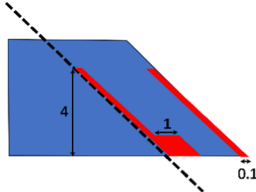
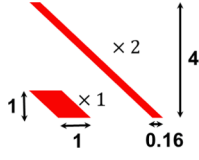
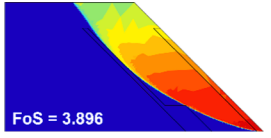


Fig. 8. Factor of Safety (FoS) and failure mode of the embankment (a) without biopolymer-treated clay and (b) with biopolymer-treated clay.

Table 1
Four layout designs with the same volume ratio of the biopolymer-treated clays.

Reinforcement type	Schematic diagram of the model	Geometry of the reinforced soil (total area 2.29 m ²)	 $u(m)$
1. Emulate ecological blanket			
2. Emulate toe reinforcement			
3. Emulate ecological blanket & toe reinforcement			
4. Inspired from topology optimisation solution			

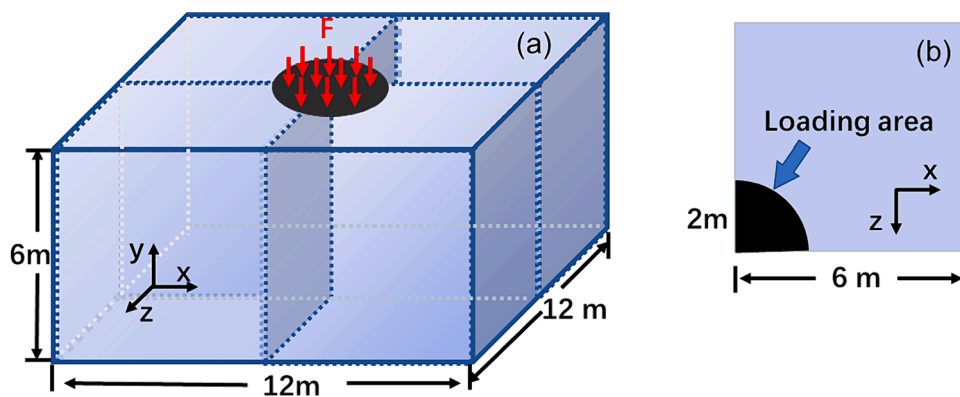


Fig. 9. An illustration of soil foundation design in 3D case: (a) Overall domain; and (b) top view of quarter section.

shown in Fig. 9. The scenario involves a cuboid domain measuring 12 m × 6 m × 12 m. All surfaces are fixed, excepted for the top surface where we intend to apply a pressure of 250 kPa to a circular region with a diameter of 2 m. When the entire domain is occupied by normal clays of a bulk unit weight of 19.6 kN/m³ and a cohesion of 30 kPa, the ultimate pressure on the circular region it can sustain is 150 kPa. This study aims to increase the bearing capacity up to 250 kPa using minimal biopolymer-treated clays. The bulk unit weight and cohesion of the biopolymer-treated clays are 27.5 kN/m³ and 230 kPa, respectively. Due to symmetry, a quarter of the domain is considered in the topology

optimisation process.

The obtained material layout obtained from the developed topology optimisation approach is shown in Fig. 10 (a). As illustrated, mesh refinement techniques are employed in the simulation to enhance computational efficiency, leading to a total computational cost of 927 s for this case. The region that should be reinforced using biopolymer-treated clays is depicted in Fig. 10 (b) and (c), with a volume of 4.54 m³ implying a volume ratio of 2.1 %.

Although such a material layout can sustain a pressure of 250 kPa on the circular region, the irregularity of the reinforced clays escalates

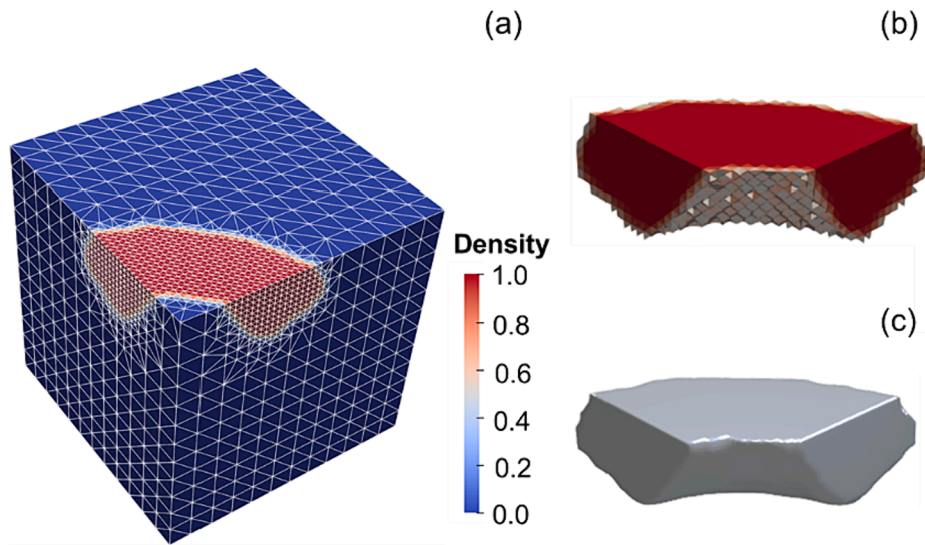


Fig. 10. An illustration of the designed soil foundation from topology optimisation: (a) material layout; (b) region with biopolymer-treated soil (before rendered); and (c) region with biopolymer-treated soil (after rendered).

Table 2
Design of soil foundations and their bearing capacity.

Topology optimisation solution	Simplified soil foundation	Bearing capacity (kPa)	Failure mode
		219	
		232	
		237	

complexity in practice. We thus simplify the design according to the topology from the simulation to alleviate the construction challenges. Three designs are illustrated in Table 2: a cylinder as the traditional circular foot, a hollow cylinder, and a design close to the shape from our topology optimisation solution. The volume of all three cases are the same, namely 4.54 m³. Simulation analysis of the bearing capacity for the three distinct designs was conducted utilising Optum G3. Although the failure mechanism of the structure is similar for these three designs, the corresponding bearing capacities differ. The findings revealed that the first scheme manifested the lowest bearing capacity of 219 kPa, merely achieving 87.6 % of the intended load magnitude. Following this, the hollow cylindrical foundation scheme, being the second approach, attained 92.5 % of the intended load magnitude. The third scheme, which closely resembles our topology-optimised design solution, comes closest to meeting the intended load magnitude, reaching 94.8 %. This suggests that, through simple modification of the topology optimisation design, we can establish a foundation that not only comes close to or even meets the required bearing capacity but is also suitable for practical construction.

5. Conclusions

This paper presents a novel three-dimensional limit analysis-based topology optimisation method tailored specifically for geostructure design. By seamlessly integrating limit analysis theory with density-based topology optimisation principles, this method enables the creation of geostructures incorporating two distinct materials, such as soils and reinforcements/foundations. Moreover, it ensures alignment of the designed geostructure's bearing capacity with the external load applied during the topology optimisation process. Validation confirms the efficacy of our approach, which has been successfully applied to various aspects of geostructure design, including embankments and soil foundations.

While designs resulting from the proposed topology optimisation method often exhibit complexity and pose challenges for practical engineering implementation, this study demonstrates the potential for further simplification. By streamlining the designs from the proposed method, we can achieve more practical and easily implementable solutions, which may not be immediate apparent. This work offers a versatile and efficient methodology for creating geostructure designs that balance material usage and structural stability.

CRedit authorship contribution statement

Xifan Li: Software, Methodology, Writing – original draft. **Xue Zhang:** Writing – review & editing, Supervision, Software, Methodology, Funding acquisition, Conceptualization. **Yujia Zhang:** Software, Methodology.

Declaration of competing interest

The authors declare that they have no known competing financial interests or personal relationships that could have appeared to influence the work reported in this paper.

Data availability

The data on optimisation algorithm are available from the corresponding author upon reasonable request. All the details necessary to

reproduce the results have been defined in the paper.

Acknowledgements

This work was supported by the New Investigator Award grant of UK Engineering and Physical Sciences Research Council (EP/V012169/1), the Royal Society International Exchanges grant (IEC/NSFC/191261) and the China Scholarship Council (CSC, No.202108420035).

References

- ApS, M., 2019. Mosek optimization toolbox for matlab. User's Guide and Reference Manual, Version 4.
- Chang, I., Lee, M., Tran, A.T.P., Lee, S., Kwon, Y.-M., Im, J., Cho, G.-C., 2020. Review on biopolymer-based soil treatment (BPST) technology in geotechnical engineering practices. *Transp. Geotech.* 24, 100385.
- Dunne, H., Martin, C., 2017. Capacity of rectangular mudmat foundations on clay under combined loading. *Géotechnique* 67 (2), 168–180.
- Duysinx, P., Bendsøe, M.P., 1998. Topology optimization of continuum structures with local stress constraints. *Int. J. Numer. Meth. Eng.* 43 (8), 1453–1478.
- Hadjiloo, E., Knutz, S., Grabe, J., 2023. Towards the saving potentials using a hybrid topology optimization: Application of a coupled deterministic and empirical approach solving a geotechnical optimization problem. *Int. J. Numer. Meth. Eng.* e7410.
- Herfelt, M.A., Poulsen, P.N., Hoang, L.C., 2019. Strength-based topology optimisation of plastic isotropic von Mises materials. *Struct. Multidiscip. Optim.* 59 (3), 893–906.
- Holmberg, E., Torstenfelt, B., Klarbring, A., 2013. Stress constrained topology optimization. *Struct. Multidiscip. Optim.* 48, 33–47.
- Kammoun, Z., Smaoui, H., 2015. A direct method formulation for topology plastic design of continua. In: Fuschl, P., Pisano, A.A., Weichert, D. (Eds.), *Direct Methods for Limit and Shakedown Analysis of Structures: Advanced Computational Algorithms and Material Modelling*. Springer International Publishing, Cham, pp. 47–63.
- Kammoun, Z., Fourati, M., Smaoui, H., 2019. Direct limit analysis based topology optimization of foundations. *Soils Found.* 59 (4), 1063–1072.
- Krabbenhöft, K., Lyamin, A.V., Sloan, S.W., 2007. Formulation and solution of some plasticity problems as conic programs. *Int. J. Solids Struct.* 44 (5), 1533–1549.
- Li, X., Zhang, X., Zhang, Y., 2023. Three-dimensional plasticity-based topology optimization with smoothed finite element analysis. *Comput. Mech.* <https://doi.org/10.1007/s00466-023-02378-9>.
- Meng, J., Zhang, X., Huang, J., Tang, H., Mattsson, H., Laue, J., 2020. A smoothed finite element method using second-order cone programming. *Comput. Geotech.* 123, 103547.
- Mourad, L., Bleyer, J., Mesnil, R., Nseir, J., Sab, K., Raphael, W., 2021. Topology optimization of load-bearing capacity. *Struct. Multidiscip. Optim.* 64 (3), 1367–1383.
- Nguyen, H.C., 2023. A mixed formulation of limit analysis for seismic slope stability. *Géotech. Lett.* 13 (1), 54–64.
- Pucker, T., Grabe, J., 2011. Structural optimization in geotechnical engineering: basics and application. *Acta Geotech.* 6, 41–49.
- Ren, G., Smith, J.V., Tang, J.W., Xie, Y.M., 2005. Underground excavation shape optimization using an evolutionary procedure. *Comput. Geotech.* 32 (2), 122–132.
- Ren, G., Zuo, Z.H., Xie, Y.M., Smith, J.V., 2014. Underground excavation shape optimization considering material nonlinearities. *Comput. Geotech.* 58, 81–87.
- Seitz, K.-F., Grabe, J., 2016. Three-dimensional topology optimization for geotechnical foundations in granular soil. *Comput. Geotech.* 80, 41–48.
- Sigmund, O., 2007. Morphology-based black and white filters for topology optimization. *Struct. Multidiscip. Optim.* 33 (4), 401–424.
- Sigmund, O., Maute, K., 2013. Topology optimization approaches: A comparative review. *Struct. Multidiscip. Optim.* 48 (6), 1031–1055.
- Smaoui, H., Kammoun, Z., 2022. Convergence of the direct limit analysis design method for discrete topology optimization. *Optim. Eng.* 23 (1), 1–24.
- Walker, J., Yu, H.-S., 2010. Analysis of the cone penetration test in layered clay. *Géotechnique* 60 (12), 939–948.
- Zhang, X., Onate, E., Torres, S.A.G., Bleyer, J., Krabbenhöft, K., 2019. A unified Lagrangian formulation for solid and fluid dynamics and its possibility for modelling submarine landslides and their consequences. *Comput. Methods Appl. Mech. Eng.* 343, 314–338.
- Zhang, X., Li, X., Zhang, Y., 2023a. A framework for plasticity-based topology optimization of continuum structures. *Int. J. Numer. Meth. Eng.* 124 (7), 1493–1509.
- Zhang, Y., Zhang, X., Nguyen, H., Li, X., Wang, L., 2023b. An implicit 3D nodal integration based PFEM (N-PFEM) of natural temporal stability for dynamic analysis of granular flow and landslide problems. *Comput. Geotech.* 159, 105434.